frontiers | Frontiers in Environmental Science

TYPE Original Research
PUBLISHED 22 December 2023
DOI 10.3389/fenvs.2023.1314536

OPEN ACCESS

EDITED BY
Liting Hao,
Beijing University of Civil Engineering and Architecture, China

REVIEWED BY
Mengjie Pu,
Wenzhou University, China
María Luisa Del Prado,
Escuela de Ingeniería y Ciencias, Campus Ciudad de México, Mexico

*CORRESPONDENCE
Jianhua Yang,
yangjh@ahut.edu.cn

RECEIVED 10 October 2023
ACCEPTED 12 December 2023
PUBLISHED 22 December 2023

CITATION
Gan X, Song Y, Liu G, Zhang H and Yang J (2023), The efficient degradation and mechanism of sulfamethoxazole using $ZnO/ZnIn_2S_4$ heterojunction under visible light.
Front. Environ. Sci. 11:1314536.
doi: 10.3389/fenvs.2023.1314536

The efficient degradation and mechanism of sulfamethoxazole using $ZnO/ZnIn_2S_4$ heterojunction under visible light

Xinhong Gan[1], Yang Song[2], Guoqiang Liu[1], Huijuan Zhang and Jianhua Yang[2]*

[1]State Environmental Protection Key Laboratory of Soil Environmental Management and Pollution Control, Nanjing Institute of Environmental Science, Ministry of Ecology and Environment (MEE) of China, Nanjing, China, [2]Anhui University of Technology, School of Energy and Environment, Maanshan, Anhui, China

We hydrothermally synthesized a flower-shaped $ZnO/ZnIn_2S_4$(ZnO/ZIS) Z-scheme heterojunction, which could decompose antibiotics efficiently. Meanwhile, the photocatalysts degradation of sulfamethoxazole (SMX) as the representative pollutant by ZnO/ZIS were studied deeply. When irradiated by a xenon lamp (500 W), ZnO/ZIS (0.20 g/L) degraded SMX (2.5 mg/L) in 6.5 h with an efficiency of 74.9%. The O_2^- and h^+ played key roles in the visible light-assisted decomposition of SMX by ZnO/ZIS, while the role of OH was supplementary. Additionally, we investigated the mechanism of the generation of active species environmentally persistent free radicals (PFRs) within the SMX degradation using ZnO/ZIS by performing computations and experimental analyses based on density functional theory. Besides, PFRs (predominantly oxygen-centered) generated during the visible light-assisted SMX degradation by ZnO/ZIS had a concentration of 10^{11} spin/mm^3. The generation of PFRs involves two major events, i.e., chemical adsorption and electron transfer. To adsorb the precursor F9a on ZnO, the energy required was −2.03 eV, and the electrons were transferred to the $ZnO/ZnIn_2S_4$ heterojunction from the precursor F9a. The PFRs only had minor negative impacts on the SMX degradation through ZnO/ZIS.

KEYWORDS

photocatalysis, sulfamethoxazole, $ZnO/ZnIn_2S_4$, heterojunction, visible light

1 Introduction

The concentration of antibiotics in water environment is becoming more and more high, which seriously threatens the health and safety of human (Khavar et al., 2022; Jiang et al., 2023; Kurade et al., 2023). Among them, sulfamethoxazole (SMX) is a sulfonamide antibiotic with great detection frequency and high concentration in water (Yang et al., 2018; Chen and Wang, 2021; Sathya et al., 2023). When the pKa values of SMX are 1.7 (amino N on the benzene ring) and 5.7 (amide N on the benzene ring), the chemical characteristics of SMX remain unchanged (Jia et al., 2023b; Su et al., 2023). These factors can increase the difficulty of SMX removal in environmental water (Zhang et al., 2023a).

Many researchers have studied photocatalytic technology because it has high degradation efficiency, generates negligible secondary pollution, and can be recycled (Song et al., 2023). The commonly available photocatalysts contain TiO_2 (Nemiwal et al., 2021), WO_3 (Khavar et al., 2022), ZnO (Nemiwal et al., 2021), CuS, MoS_2, ZnS

(You et al., 2022), CdS (Bhavsar et al., 2020), etc. Also, ZnO refers to a direct wide band gap (3.37 eV) semiconductor material and is an extensively investigated metal photocatalyst (Nemiwal et al., 2021). It is inexpensive, easy to produce, and highly stable. However, the photocatalytic decomposition of antibiotics using ZnO has certain limitations, including photo corrosion and easy recombination of photogenerated electron holes, which decreases the efficiency of the photocatalytic decomposition of pollutants. Semiconductor compounding might be performed for modifying ZnO photocatalysts, which solves the limitations of using a single catalyst. $ZnIn_2S_4$ (ZIS) has outstanding photoelectrochemical properties and an adequate band gap (~2.4 eV) (Ren et al., 2022). Generally, it is employed for hydrogen production by hydrolysis (Zhu et al., 2022), remediation of inorganic compounds (Qiu et al., 2020), degradation of organic pollutants (Zhang et al., 2022) and reduction of carbon dioxide (Zhao et al., 2022). The Z-scheme heterojunction can be formed through the integration of ZnO and ZIS, which can address issues like the short life of photogenerated electrons and poor photocatalytic efficiency. However, studies on the synthesis of flower-shaped ZnO/ZIS Z-scheme heterojunction for efficient SMX photodegradation are rare.

Photocatalytic techniques facilitate the mineralization of refractory antibiotics into small molecular substances like CO_2 and H_2O (Wang et al., 2022). It is a highly sophisticated process of energy conversion from an optical form to a chemical one. In this process, substantial free radicals or other super-reactive species are generated (Zhang et al., 2023b). Most free radicals generated are transient, whose half-lives are incredibly short (Zhao et al., 2023). These free radicals consist of hydroxyl radicals (·OH), superoxide radicals ($\cdot O_2^-$) and hydrogen peroxide radicals (·OOH), which allow the direct decomposition and mineralization of antibiotics (Xu et al., 2023). Hence, investigating the occurrence traits and the production rule of active species and free radicals during the photodegradation of antibiotics can help in assessing the efficiency of the photocatalytic system. The information can provide a theoretical foundation for developing an effective system of photocatalytic degradation in complicated scenarios.

Persistent free radicals (PFRs) refer to a novel kind of persistent and stable free radicals with a long half-life, in contrast to classic active species (Bi et al., 2022; Guo et al., 2023). An organic whole is formed involving free radical–metal ion particles, given the strong bond between metal oxide and PFRs, which can occur in the environment for a long period (Morazzoni, 2022; Zhang et al., 2023c). The identified PFRs include activated carbon (Zhang et al., 2021), atmospheric particles (e.g., $PM_{2.5}$) (He et al., 2021), biochar (Yang et al., 2016), and combustion particles (Xu et al., 2020), which are present in the atmospheric (Jia et al., 2023a), soil, and aqueous environmental media (Cheng et al., 2022). Xu et al. showed that PFRs can be generated by anthracene present on the clay mineral surface (Xu et al., 2020). Cheng et al. showed that PFRs can be produced by organic materials and transition metals in an aqueous environment (Cheng et al., 2022). During the decomposition of organic pollutants by transition metal oxide catalysts, PFRs can be produced, thus, affecting the photocatalytic event (Wang et al., 2022). The findings of these studies greatly helped in guiding the innovation and investigation of photocatalytic processes. Although several studies have investigated the mechanism and efficiency of SMX elimination using various photocatalysts, studies involving the active species and free radicals, particularly PFRs, associated with the transition metal oxide catalyst-aided decomposition of SMX are limited.

To address this issue, an innovative Z-scheme flower-shaped ZnO/ZIS heterostructure was hydrothermally fabricated by integrating ZnO and ZIS, which was applied to the typical antibiotic SMX disposal in wastewater. Using TEM, SEM, XRD, XPS, UV-vis, zeta potential, BET, photocurrent, and fluorescence techniques, the physicochemical and photoelectrochemical traits of composite ZnO/ZIS were elucidated. The optimal tentative conditions for ZnO/ZIS-aided degradation of SMX were identified, and the efficiency of the process was evaluated. The products were identified following SMX degradation until 6.5 h. We identified how humic acid (HA) and four general aqueous inorganic anions influenced the SMX degradation using ZnO/ZIS, aiming to theoretically validate the application of the photocatalyst in the actual antibiotic wastewater disposal system. The recycling capacity and stability of the photocatalyst in the degradation system were assessed. Emphasis was also placed on (i) the presence traits of PFRs, the direction of electron transfer between SMX and ZnO/ZIS, and the possible formation paths of PFRs during the degradation process of SMX; (ii) the association between degradation efficiency of SMX and the yield of PFRs, and the effects of PFRs in the course of SMX degradation; (iii) the mechanism of visible light-assisted degradation of SMX using ZnO/ZIS.

2 Experimental and theoretical methods

2.1 Chemicals

Zinc acetate dihydrate ($Zn(c)_2{\cdot}2H_2O$), Sulfamethoxazole ($C_{10}H_{11}N_3O_3S$, SMX), sodium oxalate, zinc sulfate heptahydrate ($ZnSO_4{\cdot}7H_2O$), thioacetamide (TAA), sodium hydroxide, urea ($CO(NH_2)_2$), tert butanol, hydrochloric acid, p-benzoquinone, sodium citrate dihydrate ($Na_3C_6H_5O_7{\cdot}2H_2O$), absolute ethanol, sodium phosphate, sodium bicarbonate and sodium bicarbonate, indium chloride tetrahydrate ($InCl_3{\cdot}2H_2O$) and sodium nitrate were all bought from Aladdin. Moreover, all the drugs used were of analytical grade.

2.2 Synthesis of photocatalyst

ZnO photocatalyst was made through hydrothermal calcination using the following two-step method (Nemiwal et al., 2021). Using the hydrothermal method, we produced the flower-like ZnO/ZIS further (Yang et al., 2023). The methods are stated in Supplementary Text S1.

2.3 Characterization method and analytical method

The characterization methods of ZnO/ZIS are stated in Supplementary Text S2, the experimental analysis method and

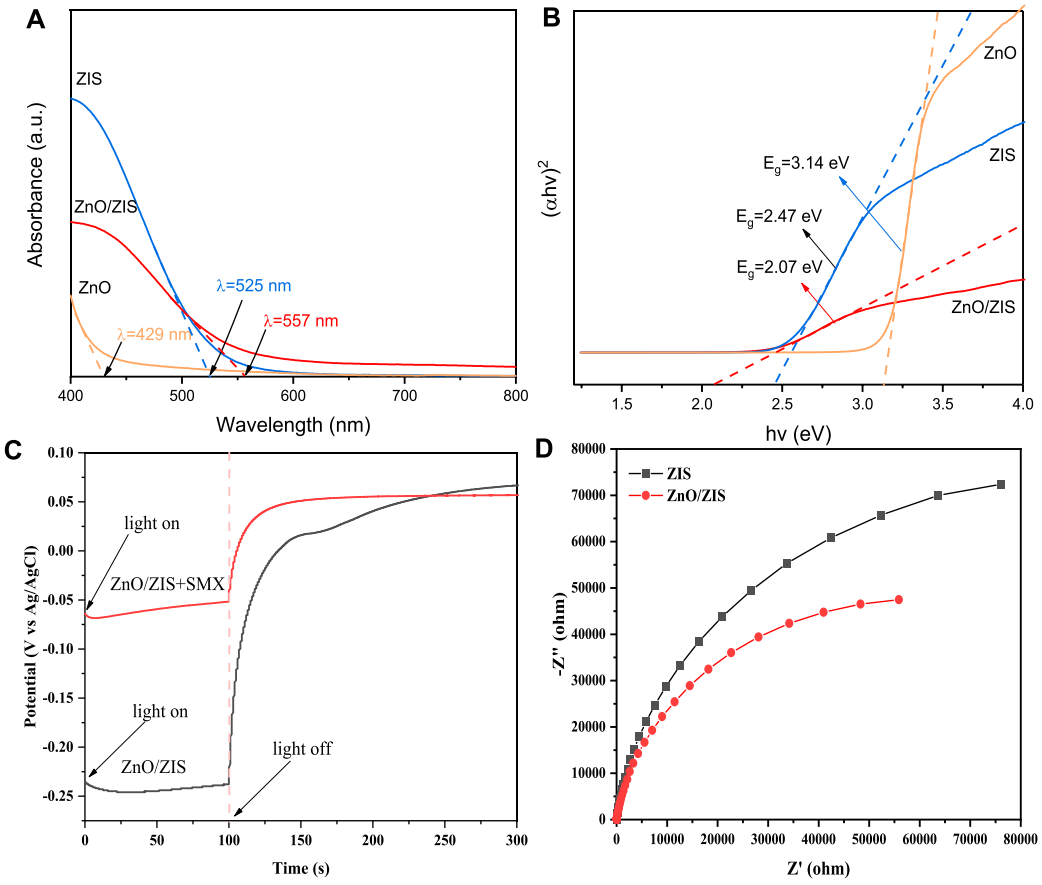

FIGURE 1
UV-vis diffuse reflectance spectra **(A)** and the band gap evaluation for linear dependence of $(Ahv)^2$ *versus* hv **(B)** of ZnO, ZIS and ZnO/ZIS; The open circuit potential between SMX and ZnO/$ZnIn_2S_4$ **(C)**; The electrochemical impedance spectroscopy of ZIS and ZnO/$ZnIn_2S_4$ **(D)**.

computational method are stated in Supplementary Text S3 and presented in Supplementary Table S1.

3 Results and discussion

3.1 Characterization results

The results regarding the analysis of SEM-EDS (Supplementary Figure S2), TEM (Supplementary Figure S2A), BET (Supplementary Figure S3) are stated in Supplementary Text S4, the analysis of XRD (Supplementary Figure S4) and XPS (Supplementary Figure S5) are stated in Supplementary Text S5, the analysis of TGA and Zeta potential (Supplementary Figure S6) are stated in Supplementary Text S6. PL and Photocurrent (Supplementary Figure S7) are stated in Supplementary Text S7. According to the analysis of UV-vis in Figures 1A, B, the band gap width is 3.14 eV for ZnO, 2.47 eV for ZIS, and 2.07 eV for ZnO/ZIS, which suggests band gap narrowing for the composite photocatalyst. This indirectly suggested that ZnO/ZIS has a higher capacity to absorb visible light. We evaluated the conduction band (CB) and valence band (VB) for ZnO and ZIS to better explain electron migration following the formation of heterojunction from the ZnO/ZIS composite. The VB and CB potentials were 3.02 and −0.12 eV, respectively, for ZnO, whereas they were 1.64 and −0.87 eV, respectively, for ZIS. The ZnO/ZIS composite exhibited a considerably better separation effect of photogenerated carriers than pure ZIS and ZnO, matching the findings of the photocurrent experiment.

To determine the direction of the transferred electrons between SMX solution and ZnO/$ZnIn_2S_4$ composite catalyst, the open circuit potential between SMX and ZnO/$ZnIn_2S_4$ was tested. The experimental methods was displayed in Supplementary Text S2, and the results was presented in Figure 1C, it showed that the electrons were transferred from ZnO/$ZnIn_2S_4$ to SMX. Besides, the electrochemical impedance spectroscopy (EIS) of ZIS and ZnO/ZIS under visible light was also conducted (Figure 1D) to characterize the advantage of ZnO/$ZnIn_2S_4$ heterojunction than pure $ZnIn_2S_4$. The results showed that the radius of ZnO/$ZnIn_2S_4$ was smaller than pure $ZnIn_2S_4$, indicating that ZnO/$ZnIn_2S_4$ has a stronger ability to separate photo generated carriers than pure $ZnIn_2S_4$.

3.2 The optimal conditions of SMX degradation by ZnO/ZIS

It was tested to be 0.5 h (see details in Supplementary Text S8) for the dark adsorption of SMX on ZnO/ZIS. To determine the best experimental situations for SMX degradation using ZnO/ZIS, the

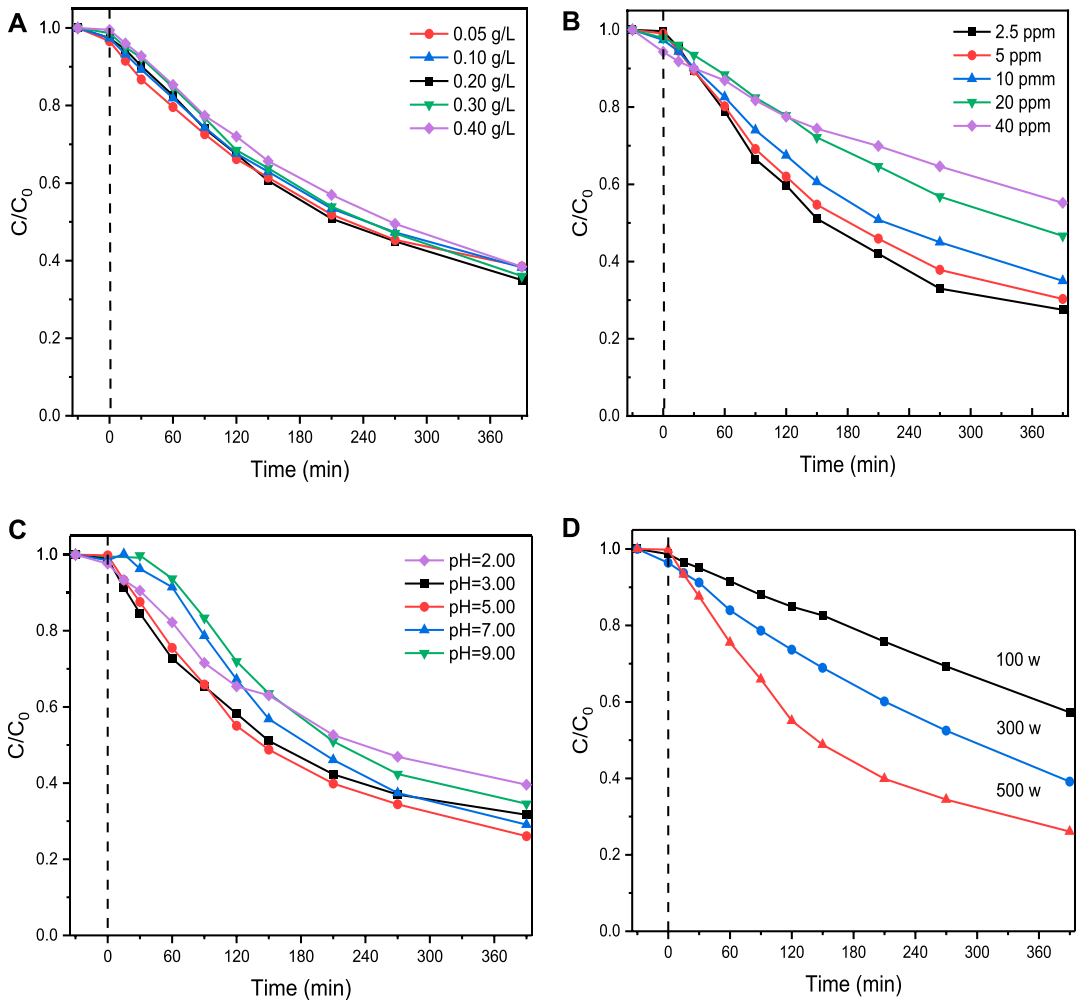

FIGURE 2
The effect of the photocatalyst amount **(A)**, degradation concentration of SMX **(B)**, pH value of the solution **(C)**, and power of simulate visible light **(D)** on SMX degradation through ZnO/ZIS.

effect of pollutant concentration, catalyst dosage, pH value and simulate visible light intensity were explored. The results are presented in Supplementary Text S9 and Figure 2. The optimal experimental conditions for the ZnO/ZIS-aided photodegradation of SMX are summarized below: an initial SMX concentration and pH of 2.5 mg/L and 5.0, respectively, a photocatalyst amount of 0.20 g/L and a xenon lamp of 500 W. All subsequent experiments were performed using these settings. The degradation efficiency of SMX using only ZnO and only $ZnIn_2S_4$ were tested under 500 W xenon lamps as control experiments (Supplementary Figure S13). When SMX degradation reached equilibrium, it was about 15% and 58% that the degradation efficiency of SMX using pure ZnO and pure $ZnIn_2S_4$ under 500 W xenon lamps, respectively. They were all lower than the degradation efficiency of SMX using ZnO/ZIS composite catalyst, implying the catalytic activity of composite ZnO/ZIS was significantly enhanced.

When xenon lamp (500 W) was used for irradiation, the efficiency of ZnO/ZIS (0.20 g/L)-aided degradation of SMX (2.5 mg/L) in 6.5 h was up to 74.9%. To further assess the ability of ZnO/ZIS to photocatalytically decompose SMX, we fitted the experimental results on the basis of the exploration of the above-mentioned influencing factors (Supplementary Figure S8). The photocatalytic degradation of SMX followed the pseudo-first-order kinetic model, which was expressed in Equation 1.

$$\ln\left(\frac{C_t}{C_0}\right) = -k_{obs}t \quad (1)$$

Here, k_{obs} indicates degradation apparent rate constant of SMX, C_0 and C_t indicate the concentration of SMX at irradiation durations of 0 and t, separately. According to the analysis, the k_{obs} value for the ZnO/ZIS-aided degradation of SMX was 0.0036 min^{-1}, following the conversion of the unit of k_{obs} into h^{-1}, the value was 0.2148 h^{-1}, y = 0.00358 x + 0.07622 (R^2 = 0.98). According to the research of koiki et al. (2021), under visible light irradiation and additional 1.5 V voltage, the removal rate of 10 mg/L SMX solution by FTO-Cu_2O was only 21%. TiO_2 was also compounded with mesoporous graphitized carbon nitrogen compounds and used for the degradation of SMX. It was found that the removal rate of SMX was 69% after continuous irradiation of simulated sunlight for 30 h under the optimal load (Koumaki et al., 2015). Therefore, ZnO/ZIS has a good degradation effect on SMX.

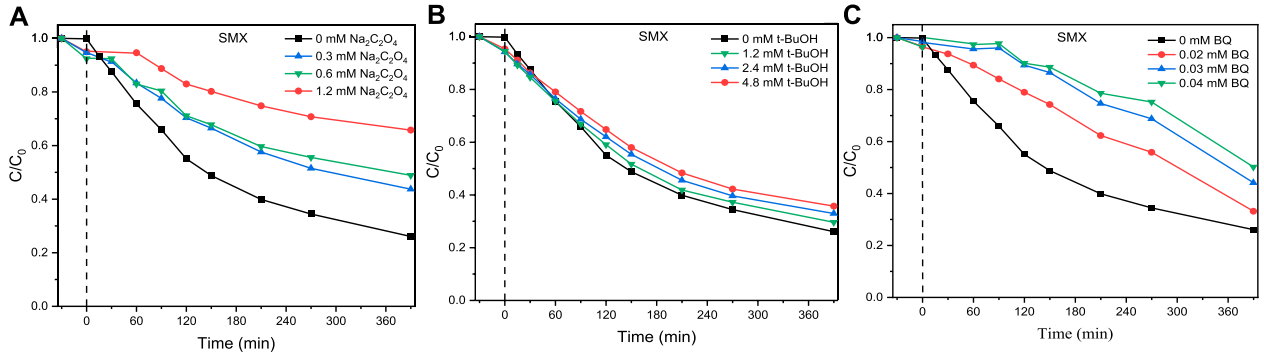

FIGURE 3
Effect of different concentrations of sodium oxalate **(A)**, tert-butanol **(B)** and p-benzoquinone **(C)** on SMX degradation using ZnO/ZIS.

3.3 Radical quenching

During the degradation process of SMX using ZnO/ZIS, a number of h^+ and transient free radicals might be engaged. Hence, a radical quenching test was conducted to identify the contribution and type of transient free radicals. As shown in Figures 3A–C, after 0.3, 0.6, and 1.2-mm $Na_2C_2O_4$ were supplemented to the degradation process in order, the efficiency of ZnO/ZIS-aided degradation of SMX was 17%, 22%, and 39%, respectively, relative to the blank group. The efficiency of ZnO/ZIS-aided degradation of SMX was 3%, 6%, and 9%, respectively, when 1.2, 2.4, and 4.8-mm tert butanol were supplemented to degradation process. When 0.02, 0.03, and 0.04-mm BQ were supplemented to the degradation system, 6%, 16%, and 24% suppression of the ZnO/ZIS-aided photodegradation of SMX was noted, respectively. By comparing the extent of restrain and the dosage of quencher, we found that O_2^- and h^+ strongly affected the photodegradation of SMXc ZnO/ZIS, while OH had a weak effect. To identify the active species in the photocatalytic reaction deeper, the EPR spectra at 0 and 10 min reaction for the $\cdot O_2^-$ and h^+ under visible light were carried out as shown in Figures 5A, B. Obviously, $\cdot O_2^-$ and h^+ free radicals were significantly produced at 10 min compared to 0 min.

The analyses of CB and VB for ZIS and ZnO were performed based on the band gap. The results are presented in the Characterization Results section. The particular route of electron transfer and the rudimentary mechanism of photodegradation were deeply analyzed. If we supposing that a type II heterojunction (shown in Figure 4A) was produced from ZIS and ZnO, So the electrons on conduction band for ZIS could be transferred to conduction band for ZnO simultaneously. Clearly, the electrons on conduction band of ZnO could not convert oxygen to superoxide radical because of E_{CB} of ZnO (−0.12 eV) was shown to be smaller than that for $O_2/\cdot O_2^-$ (−0.33 eV) (Xu et al., 2023). The E_{VB} of ZIS (1.64 eV) was lesser than that of $H_2O/\cdot OH$ (2.27 eV) and $OH^-/\cdot OH$ (2.38 eV). Thus, the h^+ on VB of ZnO unable to convert OH^-/H_2O to OH, falsifying the above-mentioned assume.

In accordance with the charge transfer route shown in Figure 4B, the electrons on conduction band of ZnO was transferred to valence band of ZIS to recombine with the hole, while the consistent h^+ and e^-were retained on the VB of ZnO and CB of ZIS. Besides, the reduction of oxygen on CB of ZIS to superoxide radical and the oxidation of OH^-/H_2O on VB of ZnO to hydroxyl radical were possible. Moreover, the above-mentioned assumptions confirmed the formation of Z-type heterojunction from ZIS and ZnO, which retained powerful redox ability while prominently enhancing the photogenerated carrier separability, thus, enhancing the efficiency of the photodegradation of SMX.

3.4 Impact of anion on the degradation of SMX by ZnO/ZIS

Water contains many ions like HCO_3^-, NO_3^- SO_4^{2-}, and PO_4^{3-}, which can affect the photocatalytic process. HA is the typical organic matter that exists in natural water and wastewater (Zhang et al., 2020). Hence, we investigated how various anions and HA affected the photodegradation of SMX (Supplementary Figure S9) to theoretically validate the application of ZnO/ZIS for antibiotic wastewater disposal. The results are shown in Supplementary Text S10. The photodegradation efficiency of SMX followed the order $SO_4^{2-} \approx HA \approx NO_3^- > HCO_3^- > PO_4^{3-}$, which indicated that NO_3^-, SO_4^{2-}, and HA have negligible effects on the photodegradation of SMX.

3.5 Determination of the degradation products

We identified nine major degradation products from the photocatalytic degradation of SMX by performing an LC-MS analysis. Based on the mass nucleus ratio (m/z) information, the nine degraded fragments were designated as F1 (96.08), F2 (98.98), F3 (114.09), F4 (124.08), F5 (139.98), F6 (155.04), F7 (270.10), F8 (275.03), and F9 (283.71). The corresponding structural formula is presented in Supplementary Figure S10 and Supplementary Table S3.

3.6 Generation of PFRs

The generation conditions for PFRs can be satisfied by the transition metal-aided photodegradation of organic contaminants.

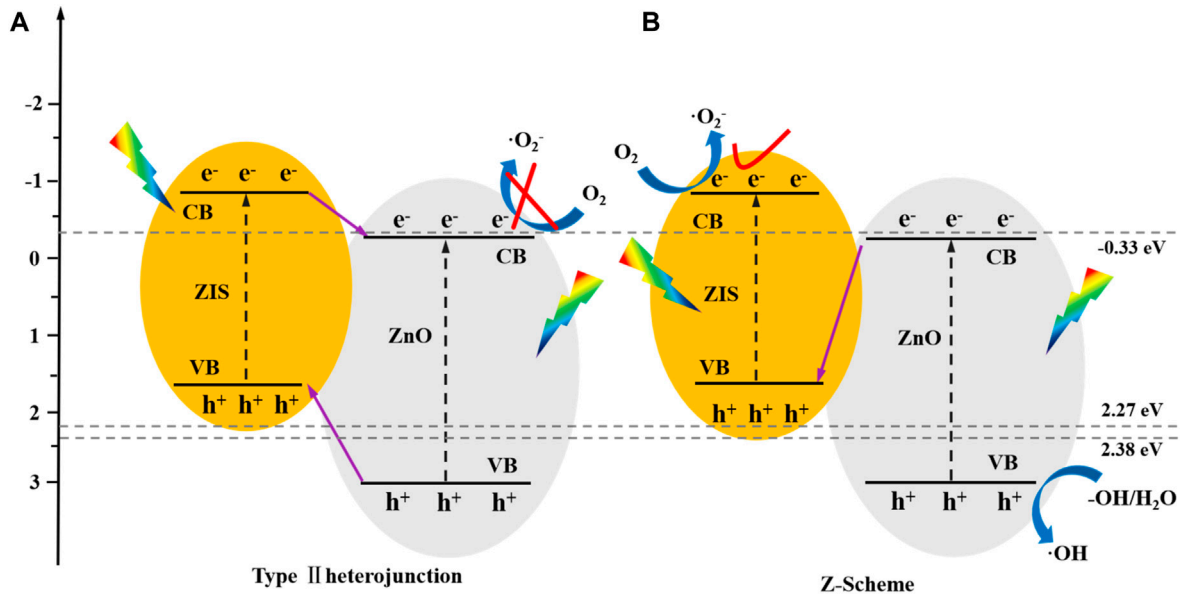

FIGURE 4
A schematic representation describing the potential mechanism for the electron deliver **(A,B)** for ZnO/ZIS photocatalyst.

Hence, we further investigated the formation and traits of PFRs in the ZnO/ZIS-aided photodegradation of SMX. The liquid samples of SMX (t = 30, 60n, 120, 210 and 270 min) at different degradation times were detected by electron paramagnetic resonance spectroscopy (EPR). As shown in Figure 5C, the g-factor of PFRs generated within he photodegradation of SMX through ZnO/ZIS ranged from 2.0044 to 2.0050, indicating that the predominant type of PFRs produced was oxygen-centered. These PFRs showed higher environmental stability than carbon-centered PFRs. The quantification of these PFRs indicated that their concentration was 10^{11} spin/mm^3, produced during the ZnO/ZIS-aided photodegradation of SMX, which was a couple of orders of magnitude less than that in the atmosphere (He et al., 2021) and soil (Tian et al., 2021). This difference occurred because the type, lifespan, concentration, and structure of PFRs are influenced by the type of precursor molecules (Li et al., 2022). Besides the impact of precursor molecules, PFRs are also suppressed to different degrees by the pH and humidity of environmental factors (Zhang et al., 2020). Thus, the low-concentration PFRs generated during the photodegradation of SMX were influenced primarily by precursor molecules, humidity, and pH.

In addition, according to D Arienzo et al., 2019, the final yield of PFRs is affected by the defects in ZnO. Hence, in this study, we investigated if intrinsic defects are present in the ZnO of the fabricated composite. Based on the findings of the photoluminescence pattern, the emission peak of ZnO was highly intense and located at 521 nm under a 376 nm excitation wavelength. Normally, it without intrinsic defects locates around 376 nm of the emission peak of pure ZnO, while the hump at 521 nm is green and ascribed to a singly charged oxygen vacancy (V_O^+). Based on the UV–vis elucidation findings, the absorption rim of pure ZnO was in the visible range at 429 nm. According to previous studies, the presence of oxygen deficiencies expands the absorption rim to the visible spectrum and enhances the usage of UV light (Nemiwal et al., 2021).

To summarize, the production of low-concentration PFRs during the photodegradation of SMX can be attributed to the effects of precursor molecules, humidity, and pH, and also to the singly charged oxygen vacancy of ZnO, which can suppress the production of PFRs.

3.7 Generation mechanism of PFRs

By determining the degradation products and studying the common types of precursor molecules, we inferred that F9a was the precursor molecule forming PFRs within the degradation of SMX. The mechanism of formation of PFRs contains two chief processes, including adsorption and electron transfer (Bi et al., 2022; Guo et al., 2023), which were determined by identifying the degradation products of SMX and analyzing the generation of the transition metal-mediated PFRs. Next, we described the mechanism of the formation of PFRs during the photodegradation of SMX from the perspectives of chemical adsorption and electron transfer.

Firstly, it involves adsorption. Based on the results about zeta potential of ZnO/ZIS photocatalyst, described in the part on characterization results, we found that the adsorption of ZnO/ZIS on SMX at pH 5.0 was a type of chemical adsorption. Some scholars have also studied the adsorption of phenols and metal elements in detail. It is generally believed that precursor molecules produce PFRs on the surface by eliminating the combination of H_2O/HCl molecules and hydroxyl groups on the metal surface (Morazzoni, 2022; Zhang et al., 2023c).

In the second step, electrons were transferred between the organic precursor molecules and the metal. To validate the

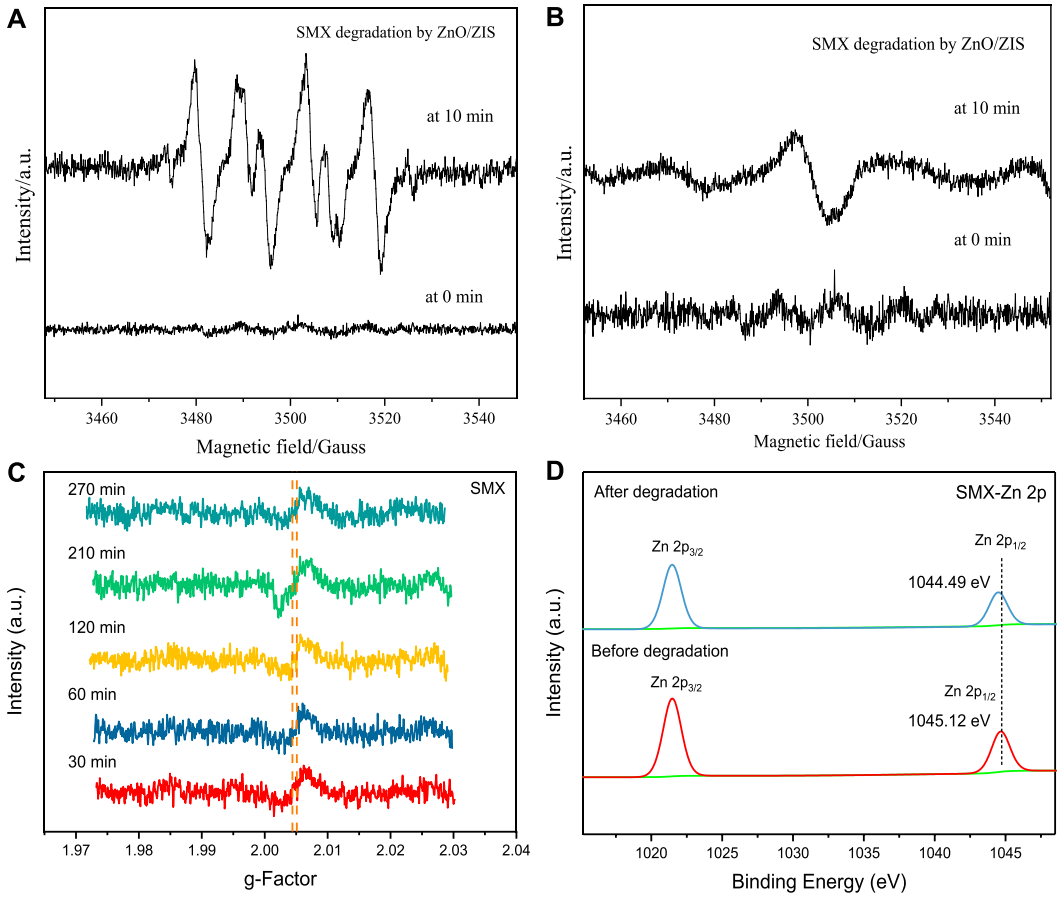

FIGURE 5
(A, B) EPR spectra at 0 min and 10 min reaction under visible light; **(C)** The EPR signal created in the ZnO/ZIS-aided photodegradation of SMX. Conditions: $[SMX]_0$ = 2.5 ppm, pH = 5.0, 0.20 g/L dosage, room temperature, 300 W; **(D)** XPS patterns of Zn initial and following the photodegradation of SMX through ZnO/ZIS.

direction of electron transfer, XPS analysis was performed on Zn elements of ZnO/ZIS in front and behind the SMX photodegradation. The location of Zn $2p_{1/2}$ orbital before and after the degradation of SMX moved from 1,045.12 eV to 1,044.49 eV (Figure 5D), suggesting that the Zn $2p_{1/2}$orbital shifted by 0.63 eV after SMX photodegradation. The change indicated SMX was effectively degraded, within the generation of PFRs that e^- were diverted from precursor substance to Zn^{2+}.

Figure 6A displays the above-mentioned speculated mechanism of the generation of PFRs within SMX degradation using ZnO/ZIS. The product F10 formed when the hydroxyl group was adjacent to -N=O on the benzene ring, which may also be at the other three positions. Only one position is listed in Figure 6A to illustrate the process of the formation of PFRs. The chemical formula of F10 was found to be $C_{20}H_{14}N_6O_9S_2$, and its mass nucleus ratio was m/z = 546. By comparing with the results of the LC-MS analysis, we found that there were mass spectrograms with similar mass composition ratios (Supplementary Figure S11).

The absolute energy ($E_{(g)}$) of F9a gas molecules, the $E_{(g)}$, and the adsorption energy (E_{ads}) of F9a on the surface of the ZnO(001)/$ZnIn_2S_4$(102) heterojunction were measured using the DFT method. The findings of the analysis are presented in Supplementary Table S4. The F9a isolated molecule had an $E_{(g)}$ value of −185.684 eV; the $E_{(g)}$ of F9a was −1,085.751 on the side of ZnO and −1,086.454 eV on the side of $ZnIn_2S_4$. The E_{ads} of F9a was −2.03 on the side of ZnO and −1.65 eV on the side of $ZnIn_2S_4$. The E_{ads} values of F9a on both sides [ZnO(001)/$ZnIn_2S_4$(102)] were negative, suggesting the adsorbability of precursor F9a on the heterojunction and the thermodynamic stability of the post-adsorption system. A more negative value of E_{ads} indicated stronger adsorbability. These findings also confirmed that precursor F9a was adsorbed on the ZnO/$ZnIn_2S_4$ heterojunction.

In addition to the measured data, theoretical calculations about the differential charge density were also verified, it of F9a on the $ZnIn_2S_4$ side and the ZnO side were computed for the formation of PFRs deeply (Figure 7). Clearly, the blue and yellow isosurfaces were consistent with the depletion and accumulation of electrons. By combining the data on adsorption energy, the E_{ads} of F9a on the $ZnIn_2S_4$ side was found to be −2.03 eV. It was larger than the E_{ads} of F9a on the ZnO side. Additionally, we also found that F9a was adsorbed closest to the upper surface (Figure 7). These findings matched the results of XPS, indicating that the electrons were delivered from precursor F9a to ZnO/$ZnIn_2S_4$.

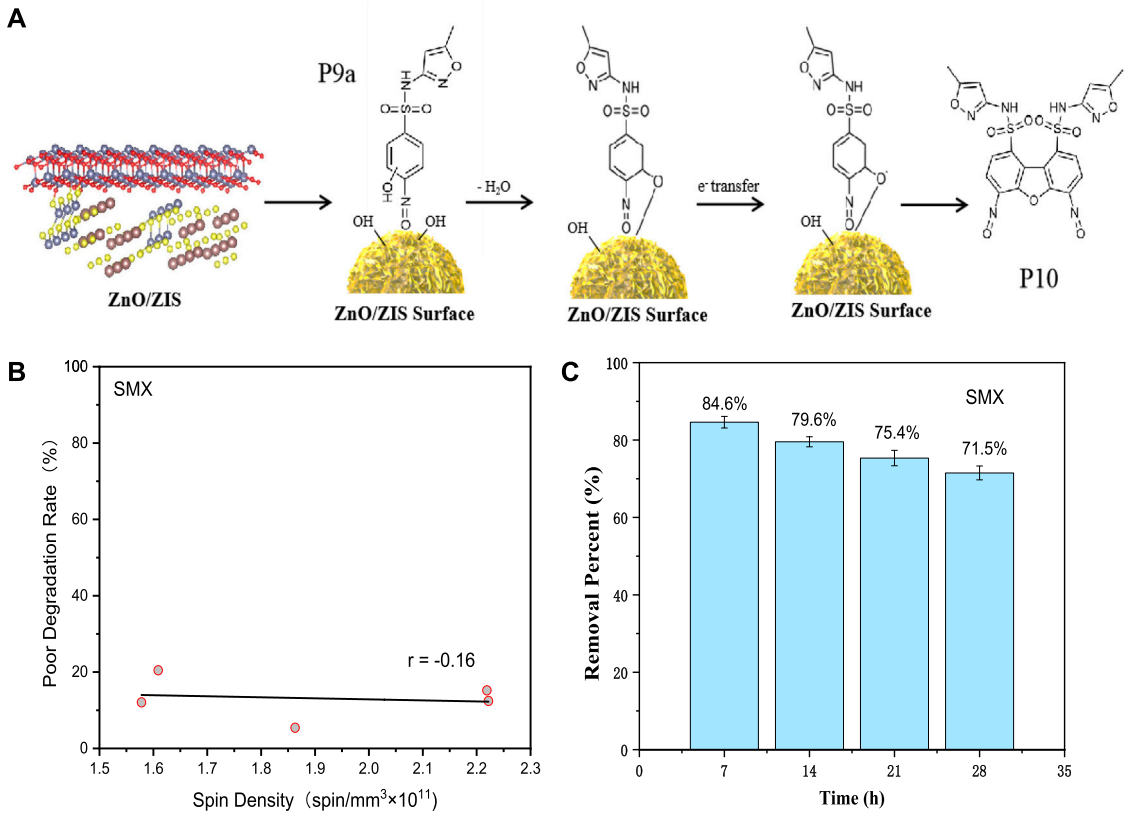

FIGURE 6
(A) A diagrammatic representation of the mechanism of formation of PFRs in the ZnO/ZIS-aided degradation of SMX. **(B)** The correlation between content of PFRs and SMX degradation rate using ZnO/ZIS composite photocatalyst. **(C)** Recycled use of ZnO/ZIS photocatalytic degradation of SMX. Condition: $[SMX]_0$ = 2.5 mg/L, 0.20 g/L dosage, pH = 5.0, 500 W, 30°C.

3.8 Effects of PFRs on the photodegradation of SMX

Although PFRs were detected during the photodegradation of SMX and the mechanism of formation of PFRs was speculated, we did not know how the PFRs affected the photodegradation process. Hence, we quantified the changes in the concentration of EPFR at varying instances and determined the correlation between the difference in degradation efficiency and the concentration of EPFR. The abscissa in Figure 6B represents the concentration of PFRs [spin/mm ($\times 10^{11}$)]. *Y*-axis represents the difference in degradation rate of SMX, which can be determined using Equation 2.

$$R(\%) = R_2\text{-}R_1 \quad (2)$$

Here, R_1 and R_2 indicate removal efficiency of SMX at different time, separately, and $time_1$ is smaller than $time_2$. A weak negative correlation was recorded between the concentration of PFRs and the degradation efficiency difference of SMX, which indicated that the inhibitory effect of PFRs on the degradation of SMX was weak. On the one hand, this may be because the concentration of PFRs is not very high in water. On the other hand, the number of precursor molecules P9a may be limited, and further transformation to F10 may also be affected.

The result of open circuit potential between SMX and ZnO/$ZnIn_2S_4$ was presented in Figure 1C, it showed that the electrons were transferred from ZnO/$ZnIn_2S_4$ to SMX. This result was opposite to the direction of electron transfer during the formation of persistent free radicals between ZnO/$ZnIn_2S_4$ and precursor F9a. As stated in the above results, a weak negative correlation was recorded between the concentration of PFRs and the degradation efficiency difference of SMX, which indicated that the inhibitory effect of PFRs on the degradation of SMX was weak. Therefore, the result of the opposite direction of electron transfer of SMX and precursor F9a to ZnO/$ZnIn_2S_4$ was reasonable.

3.9 Conjecture of degradation pathways

Based on the above derivation information on the degradation fragment, the probable route of SMX degradation through ZnO/ZIS can be inferred. As displayed in Figure 8, upon disconnecting of C-N bond to form F1, SMX molecule is attacked by active species, and the oxidation of amino groups on the benzene ring transforms into F9a. The formation of F2 is caused by the fracture of the N-S bond on the SMX molecule and accompanied by the production of F6. The breaking of the N-S bond in F9a will also lead to the generation of F2. F2 is further attacked by active species to generate F3, and F7 is also produced by the hitting of active species on SMX molecules. F8 is considered to be the sodium salt of SMX. F9b is the result of active species attacking the amino group on the benzene ring and oxidizing it to nitro. Then, the C-S

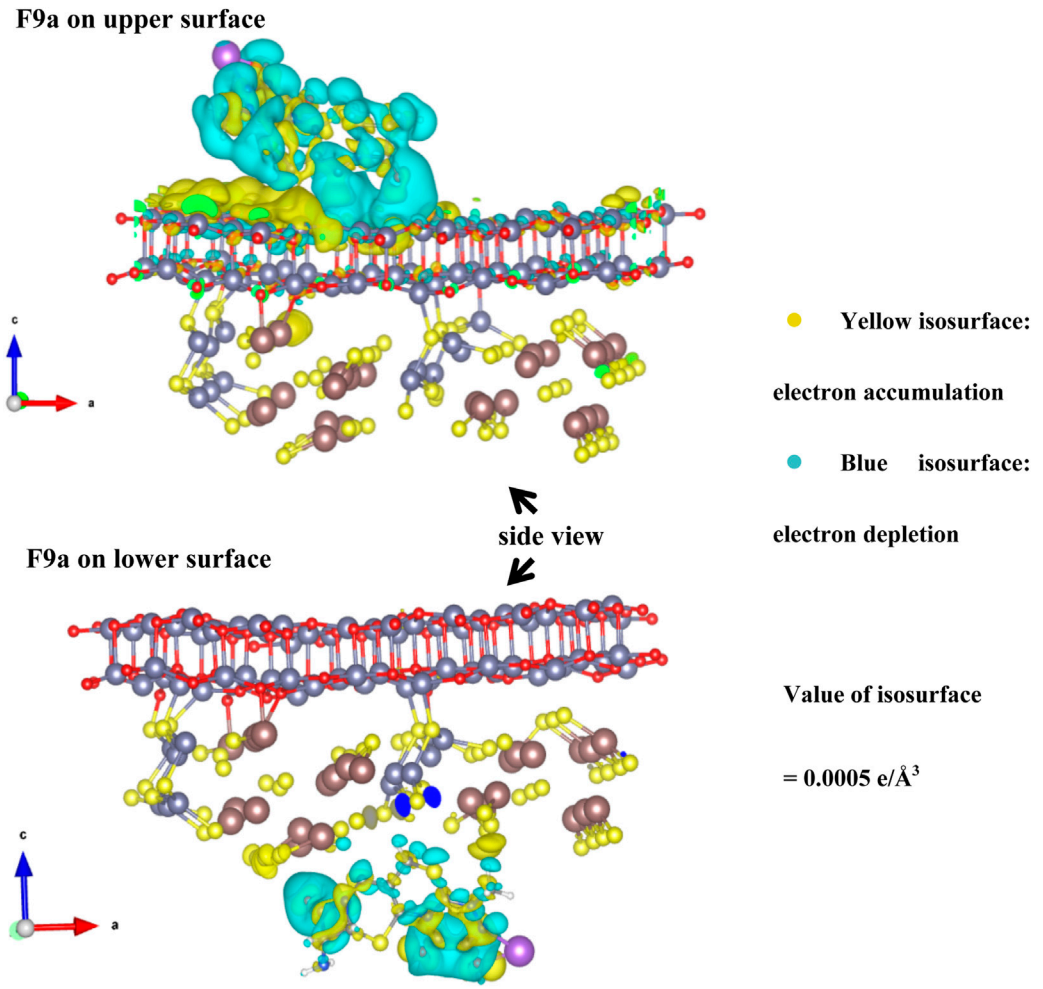

FIGURE 7
The results of the DFT-based differential charge density analysis for P9a on ZnO/ZIS.

bond breaks to form F4, and F4 is further assaulted by active species to become F5. According to the description of the generation mechanism of PFRs, the participation of PFRs leads to the formation of F10.

3.10 Underlying mechanism of degradation process

The information of radical quenching test showed that $\cdot O_2^-$ and h^+ strongly influenced the visible light-assisted degradation of SMX by ZnO/ZIS, while OH had a negligible impact on the reaction system. Upon analyzing the role of PFRs in the photodegradation of SMX, we found that the PFRs had a non-significant inhibitory effect on the photodegradation process. Hence, the mechanism of the ZnO/ZIS-aided photocatalytic degradation of SMX involves two major parts. In the first part, $\cdot O_2^-$ produced on the CB of ZIS, ·OH scarcely generated on the VB of ZnO, and the hole facilitate the SMX photodegradation into small molecules like H_2O and CO_2 during photocatalytic degradation. The second part involves the low-concentration PFRs generated during the ZnO/ZIS-aided photodegradation of SMX, which weakly inhibit the photodegradation process.

3.11 TOC, stability, and reusability test

Within the SMX degradation, the TOC alteration can reflect the extent of completely degraded to carbon dioxide and water of SMX. Thus, we measured the TOC of SMX degraded using ZnO/ZIS after 6.5 h to get the mineralization rate (Supplementary Text S11 and Supplementary Figure S12). For assessing the constancy of ZnO/ZIS photocatalyst, we determined the occurrence rate for Zn and In metal ion after SMX degradation by ZnO/ZIS; Supplementary Table S5 presents the corresponding results. With the purpose of determining the feasibility of using ZnO/ZIS, we assessed the reusability and stability of the photocatalyst when the experimental parameters were optimal. After the 6.5 h photodegradation of SMX, the recycling and reusing of ZnO/ZIS photocatalyst was performed via a series of operations. As shown in Figure 6C, we repeated the above-mentioned process was four times. The fourth degradation efficiency of SMX decreased by 13.1% compared to the first one, the average degradation efficiency of each cycle experiment decreased by about 4.36%. There are two main reasons for this result. One is the loss of catalyst quality during operation, including washing and drying, which is also the main reason for the decrease of SMX degradation efficiency. The other is that the active sites

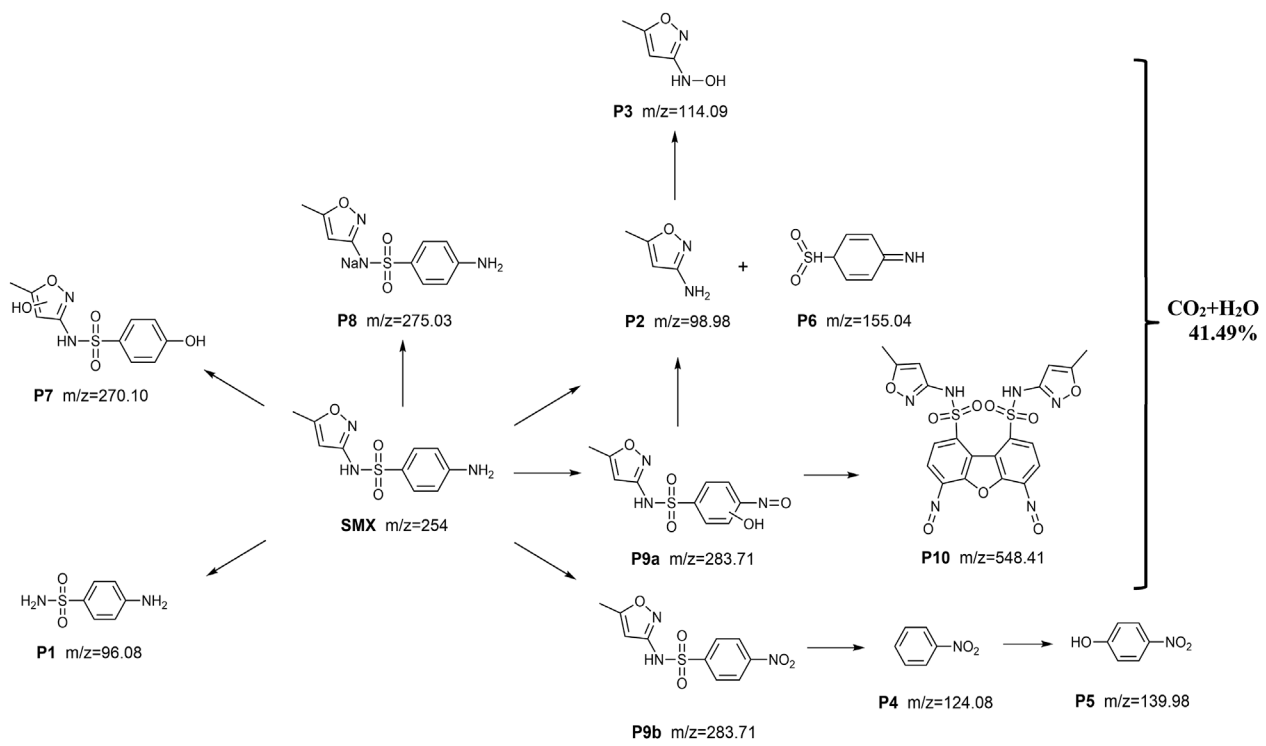

FIGURE 8
Possible degradation pathways of ZnO/ZIS degradation of SMX in aqueous solution under visible light conditions. Conditions: pH = 5.0, $[SMX]_0$ = 2.5 mg/L, 0.20 g/L ZnO/ZIS, 500 W, 25°C ± 0.5°C.

on the catalyst surface were occupied during SMX degradation, leading to a decrease in subsequent degradation efficiency.

4 Conclusion

This study had three major contributions. First, here, we developed an innovative flower-shaped Z-scheme ZnO/ZIS heterostructure that can efficiently photodegrade antibiotics. The process avoids the problems related to the use of a single catalyst and also allows prominent heterojunction formation, significantly high visible light utilization, as well as considerably improved photogenerated carrier separability. Second, we provided new information concerning the mechanism of degradation of SMX through the ZnO/ZIS photocatalytic system by analyzing the persistent and transient free radicals. Finally, we elucidated the process of formation and the effects of PFRs during the ZnO/ZIS-aided photocatalytic decomposition of SMX.

We evaluated the influencing factors, degradation efficiency, as well as the degradation mechanism of SMX through ZnO/ZIS. We found that O_2^- and h^+ strongly affected the degradation of SMX; however, ·OH had a weak function in the process. Other results suggested that ZnO/ZIS could preferably mineralize SMX. ZnO/ZIS was quite stable and reusable.

As shown in the system, within the SMX degradation through ZnO/ZIS under visible-light irradiation, the PFRs produced were centered on oxygen atoms. The concentration of the PFRs was around 10^{11} (unit: spin/mm^3). Additionally, the production of PFRs involved two major processes, one involved the chemical adsorption between precursor molecules and Zn^{2+} and the other involved the transfer of electrons to Zn^{2+} from the precursor molecules. The negative effects of the PFRs on the visible light-assisted degradation of SMX by ZnO/ZIS were weak. This work provides data support and reference for the study of persistent free radicals in aqueous photocatalytic system, future studies are warranted to promote the development and application of photocatalytic system for the treatment of wastewater.

Data availability statement

The original contributions presented in the study are included in the article/Supplementary Material, further inquiries can be directed to the corresponding author.

Author contributions

XG: Writing–original draft, Formal Analysis, Investigation. YS: Data curation, Formal Analysis, Investigation, Writing–original draft. GL: Conceptualization, Formal Analysis, Methodology, Writing–original draft. HZ: Formal Analysis, Investigation, Writing–original draft. JY: Conceptualization, Writing–original draft, Writing–review and editing.

Funding

The author(s) declare financial support was received for the research, authorship, and/or publication of this article. The authors

gratefully thank the open fund of State Key Laboratory of Pollution Control and Resource Reuse (No. PCRRF210010), key projects of Anhui Provincial Department of Education of China (No. KJ 2021A0383), and the open fund of Engineering Research Center of Biofilm Water Purification and Utilization Technology of Ministry of Education (Nos. BWPU2020KF06 and BWPU2020KF07).

Conflict of interest

The authors declare that the research was conducted in the absence of any commercial or financial relationships that could be construed as a potential conflict of interest.

Publisher's note

Supplementary material

The Supplementary Material for this article can be found online at: https://www.frontiersin.org/articles/10.3389/fenvs.2023.1314536/full#supplementary-material

References

Bhavsar, K. S., Labhane, P. K., Dhake, R. B., and Sonawane, G. H. (2020). Solvothermal synthesis of activated carbon loaded CdS nanoflowers: boosted photodegradation of dye by adsorption and photocatalysis synergy. *Chem. Phys. Lett.* 744, 137202. doi:10.1016/j.cplett.2020.137202

Bi, D. M., Huang, F. P., Jiang, M., He, Z. S., and Lin, X. N. (2022). Effect of pyrolysis conditions on environmentally persistent free radicals (EPFRs) in biochar from co-pyrolysis of urea and cellulose. *Sci. Total Environ.* 805, 150339. doi:10.1016/j.scitotenv.2021.150339

Chen, H., and Wang, J. L. (2021). Degradation of sulfamethoxazole by ozonation combined with ionizing radiation. *J. Hazard. Mater.* 407, 124377. doi:10.1016/j.jhazmat.2020.124377

Cheng, P. F., Zhao, X. Q., El-Ramady, H., Elsakhawy, T., Waigi, M. G., and Ling, W. T. (2022). Formation of environmentally persistent free radicals from photodegradation of triclosan by metal oxides/silica suspensions and particles. *Chemosphere* 290, 133322. doi:10.1016/j.chemosphere.2021.133322

D Arienzo, M., Mostoni, S., Crapanzano, R., Cepek, C., Di Credico, B., Fasoli, M., et al. (2019). Insight into the influence of ZnO defectivity on the catalytic generation of environmentally persistent free radicals in ZnO/SiO_2 systems. *J. Phys. Chem. C* 123 (35), 21651–21661. doi:10.1021/acs.jpcc.9b06900

Guo, L. J., Zhao, L. M., Tang, Y. L., Zhou, J. F., and Shi, B. (2023). Chrome shaving-derived biochar as efficient persulfate activator: Ti-induced charge distribution modulation for $^1O_2$ dominated nonradical process. *Sci. Total Environ.* 862, 160838. doi:10.1016/j.scitotenv.2022.160838

He, Q. Y., Guo, Y., Mao, H. Y., Chen, H., Li, Y., Zhang, W. F., et al. (2021). Ultrasonic-assisted solvent extraction method for the determination of environmentally persistent free radicals in $PM_{2.5}$. *Chem. Lett.* 50 (7), 1368–1371. doi:10.1246/cl.210097

Jia, S. M., Wang, D. Q., Liu, L. Y., Zhang, Z. F., and Ma, W. L. (2023a). Size-resolved environmentally persistent free radicals in cold region atmosphere: implications for inhalation exposure risk. *J. Hazard. Mater.* 443, 130263. doi:10.1016/j.jhazmat.2022.130263

Jia, Y. F., Yang, K. L., Zhang, Z. S., Gu, P., Liu, S. G., Li, M. M., et al. (2023b). Heterogeneous activation of peroxymonosulfate by magnetic hybrid $CuFe_2O_4$@N-rGO for excellent sulfamethoxazole degradation: interaction of $CuFe_2O_4$ with N-rGO and synergistic catalytic mechanism. *Chemosphere* 313, 137392. doi:10.1016/j.chemosphere.2022.137392

Jiang, R. R., Lu, G. H., Dang, T. J., Wang, M., Liu, J. C., Yan, Z. H., et al. (2023). Hydrogen-bond based charge bridge in a heterojunction system for the synergistic degradation and detoxification of two PPCPs. *Chem. Eng. J.* 454, 140018. doi:10.1016/j.cej.2022.140018

Khavar, A. H. C., Khazaee, Z., and Mahjoub, A. (2022). Electron flux at the Schottky junction of Bi NPs and WO_3-supported g-C_3N_4: an efficient ternary S-scheme catalyst for removal of fluoroquinolone-type antibiotics from water. *Environ. Sci. Pollut. Res.* 30, 18461–18479. doi:10.1007/s11356-022-23370-5

Koiki, B. A., Orimolade, B. O., Zwane, B. N., Nkwachukwu, O. V., Muzenda, C., Nkosi, D., et al. (2021). The application of FTO-Cu_2O/Ag_3PO_4 heterojunction in the photoelectrochemical degradation of emerging pharmaceutical pollutant under visible light irradiation. *Chemosphere* 266, 129231. doi:10.1016/j.chemosphere.2020.129231

Koumaki, E., Mamais, D., Noutsopoulos, C., Nika, M. C., Bletsou, A. A., Thomaidis, N. S., et al. (2015). Degradation of emerging contaminants from water under natural sunlight: the effect of season, pH, humic acids and nitrate and identification of photodegradation by-products. *Chemosphere* 138, 675–681. doi:10.1016/j.chemosphere.2015.07.033

Kurade, M. B., Mustafa, G., Zahid, M. T., Awasthi, M. K., Chakankar, M., Pollmann, K., et al. (2023). Integrated phycoremediation and ultrasonic-irradiation treatment (iPUT) for the enhanced removal of pharmaceutical contaminants in wastewater. *Chem. Eng. J.* 455, 140884. doi:10.1016/j.cej.2022.140884

Li, X. T., Zhao, H. X., Qu, B. C., and Tian, Y. (2022). Photoformation of environmentally persistent free radicals on particulate organic matter in aqueous solution: role of anthracene and formation mechanism. *Chemosphere* 291, 132815. doi:10.1016/j.chemosphere.2021.132815

Morazzoni, F. (2022). Reexamining the formation of environmentally persistent free radicals from aromatic molecules on metal oxides. *Catal. Lett.* 152 (8), 2235–2238. doi:10.1007/s10562-021-03830-2

Nemiwal, M., Zhang, T. C., and Kumar, D. (2021). Recent progress in g-C_3N_4, TiO_2 and ZnO based photocatalysts for dye degradation: strategies to improve photocatalytic activity. *Sci. Total Environ.* 767, 144896. doi:10.1016/j.scitotenv.2020.144896

Qiu, J. H., Li, M., Xu, J., Zhang, X. F., and Yao, J. F. (2020). Bismuth sulfide bridged hierarchical Bi_2S_3/BiOCl@$ZnIn_2S_4$ for efficient photocatalytic Cr(VI) reduction. *J. Hazard. Mater.* 389, 121858. doi:10.1016/j.jhazmat.2019.121858

Ren, Y. J., Foo, J. J., Zeng, D. Q., and Ong, W. J. (2022). $ZnIn_2S_4$-based nanostructures in artificial photosynthesis: insights into photocatalytic reduction toward sustainable energy production. *Small Struct.* 3 (11), 2200017. doi:10.1002/sstr.202270033

Sathya, P. M., Mohan, H., Venkatachalam, J., and Seralathan, K. K. (2023). A hybrid technique for sulfamethoxazole (SFM) removal using Enterobacter hormaechei HaG-7: bio-electrokinetic degradation, pathway and toxicity. *Chemosphere* 313, 137485. doi:10.1016/j.chemosphere.2022.137485

Song, Y. F., Li, Y. J., Chen, X. M., Meng, C. C., Ma, S. F., Li, T. M., et al. (2023). Simultaneous degradation and separation of antibiotics in sewage effluent by photocatalytic nanofiltration membrane in a continuous dynamic process. *Water Res.* 229, 119460. doi:10.1016/j.watres.2022.119460

Su, Q. X., Huang, S. J., Zhang, H., Wei, Z. S., and Ng, H. Y. (2023). Abiotic transformations of sulfamethoxazole by hydroxylamine, nitrite and nitric oxide during wastewater treatment: kinetics, mechanisms and pH effects. *J. Hazard. Mater.* 444, 130328. doi:10.1016/j.jhazmat.2022.130328

Tian, H., Wang, Z., Zhu, T., Yang, C., Shi, Y., and Sun, Y. (2021). Degradation prediction and products of polycyclic aromatic hydrocarbons in soils by highly active bimetals/AC-activated persulfate. *ACS ES&T Eng.* 1 (8), 1183–1192. doi:10.1021/acsestengg.1c00063

Wang, Z. W., Xu, P. A., Wang, H., Almatrafi, E., Zhou, C. Y., He, Y. Z., et al. (2022). Environmentally persistent free radicals in bismuth-based metal-organic layers derivatives: photodegradation of pollutants and mechanism unravelling. *Chem. Eng. J.* 430, 133026. doi:10.1016/j.cej.2021.133026

Xu, J., Dai, Y. C., Shi, Y. F., Zhao, S., Tian, H. X., Zhu, K. C., et al. (2020). Mechanism of Cr(VI) reduction by humin: role of environmentally persistent free radicals and reactive oxygen species. *Sci. Total Environ.* 725, 138413. doi:10.1016/j.scitotenv.2020.138413

Xu, L. Y., Dai, R., Yang, J., Yan, J. F., Zhang, Y. Y., Dai, Y., et al. (2023). A novel S-scheme g-C_3N_4/$Mn(VO_3)_2$ heterojunction photocatalyst for its superior photocatalytic degradation of broad-spectrum antibiotics. *J. Alloys Compd.* 936, 168163. doi:10.1016/j.jallcom.2022.168163

Yang, C. W., Tsai, L. L., and Chang, B. V. (2018). Anaerobic degradation of sulfamethoxazole in mangrove sediments. *Sci. Total Environ.* 643, 1446–1455. doi:10.1016/j.scitotenv.2018.06.305

Yang, J., Lu, F., Li, Z., Meng, G., Jia, Y., Jiang, Y., et al. (2023). Insights into the formation of environmentally persistent free radicals during photocatalytic degradation processes of ceftriaxone sodium by ZnO/$ZnIn_2S_4$. *Chemosphere* 314, 137618. doi:10.1016/j.chemosphere.2022.137618

Yang, J., Pan, B., Li, H., Liao, S. H., Zhang, D., Wu, M., et al. (2016). Degradation of p-Nitrophenol on biochars: role of persistent free radicals. *Environ. Sci. Technol.* 50 (2), 694–700. doi:10.1021/acs.est.5b04042

You, J. Y., Liu, C., Feng, X., Lu, B. W., Xia, L., and Zhuang, X. P. (2022). *In situ* synthesis of ZnS nanoparticles onto cellulose/chitosan sponge for adsorption-photocatalytic removal of Congo red. *Carbohydr. Polym.* 288, 119332. doi:10.1016/j.carbpol.2022.119332

Zhang, B., He, Y. K., Shi, W. X., Liu, L. J., Li, L., Liu, C., et al. (2023a). Biotransformation of sulfamethoxazole (SMX) by aerobic granular sludge: removal performance, degradation mechanism and microbial response. *Sci. Total Environ.* 858, 159771. doi:10.1016/j.scitotenv.2022.159771

Zhang, G. P., Wu, H., Chen, D. Y., Li, N. J., Xu, Q. F., Li, H., et al. (2022). A mini-review on $ZnIn_2S_4$-Based photocatalysts for energy and environmental application. *Green Energy and Environ.* 7 (2), 176–204. doi:10.1016/j.gee.2020.12.015

Zhang, X. J., Zhu, X. B., Li, H., Wang, C. H., and Zhang, T. T. (2023b). Combination of peroxymonosulfate and Fe(VI) for enhanced degradation of sulfamethoxazole: the overlooked roles of high-valent iron species. *Chem. Eng. J.* 453, 139742. doi:10.1016/j.cej.2022.139742

Zhang, Y. Z., He, R., and Zhao, J. (2023c). Removal mechanism of tetracycline-Cr(VI) combined pollutants by different S-doped sludge biochars: role of environmentally persistent free radicals. *Chemosphere* 317, 137856. doi:10.1016/j.chemosphere.2023.137856

Zhang, Y. Z., Xu, M. Q., Liu, X. K., Wang, M., Zhao, J., Li, S. Y., et al. (2021). Regulation of biochar mediated catalytic degradation of quinolone antibiotics: important role of environmentally persistent free radicals. *Bioresour. Technol.* 326, 124780. doi:10.1016/j.biortech.2021.124780

Zhang, Y. Z., Yin, M. C., Sun, X. D., and Zhao, J. (2020). Implication for adsorption and degradation of dyes by humic acid: light driven of environmentally persistent free radicals to activate reactive oxygen species. *Bioresour. Technol.* 307, 123183. doi:10.1016/j.biortech.2020.123183

Zhao, C., Meng, L. H., Chu, H. Y., Wang, J. F., Wang, T. Y., Ma, Y. H., et al. (2023). Ultrafast degradation of emerging organic pollutants via activation of peroxymonosulfate over Fe_3C/Fe@N-C-x: singlet oxygen evolution and electron-transfer mechanisms. *Appl. Catal. B-Environmental* 321, 122034. doi:10.1016/j.apcatb.2022.122034

Zhao, Y. M., Chen, Y. J., Du, L. Z., Wang, Q., Liu, X., Li, L. G., et al. (2022). Fabrication of size-controlled hierarchical ZnS@$ZnIn_2S_4$ heterostructured cages for enhanced gas-phase CO_2 photoreduction. *J. Colloid Interface Sci.* 605, 253–262. doi:10.1016/j.jcis.2021.07.093

Zhu, C. Z., He, Q. Y., Wang, W. K., Du, F., Yang, F., Chen, C. X., et al. (2022). S-scheme photocatalysis induced by $ZnIn_2S_4$ nanoribbons-anchored hierarchical CeO_2 hollow spheres for boosted hydrogen evolution. *J. Colloid Interface Sci.* 620, 253–262. doi:10.1016/j.jcis.2022.04.024